Astron. Astrophys. 284, 285–299 (1994)

ASTRONOMY
AND
ASTROPHYSICS

Isothermal elliptical gravitational lens models

R. Kormann*, P. Schneider, and M. Bartelmann

Max-Planck-Institut für Astrophysik, Postfach 1523, D-85740 Garching, Germany

Received 10 September 1993 / Accepted 30 September 1993

Abstract. Gravitational lens models for observed lensing systems are often based on quasi-elliptical lenses. The use of elliptical mass distributions is motivated by observations of galaxies and by the assumption that mass follows light. Elliptical mass distributions are also expected on theoretical grounds. On the other hand, since elliptical matter distributions are in general more difficult to handle, quasi-elliptical lens models, in which the isopotential curves are ellipses or in which an external shear component is added onto a spherical deflector, are often used for model fitting or for statistical lens studies. However, elliptical potentials correspond to unphysical matter distributions if the ellipticity is large. In this paper we derive explicit lens equations for a special type of elliptical matter distributions, the 'isothermal' ellipsoids. Their matter distribution forms a natural generalization of isothermal spheres, one of the most commonly used models in lens theory. We consider the singular and the non-singular case. For both, the deflection angle is derived in closed form, and it is particularly simple for the singular case. The lens equation in the singular case can be reduced to a one-dimensional equation, making its solution particularly easy. We derive the critical curves and caustics of these isothermal elliptical lens models and obtain a complete classification of the topologies of the critical curves and the caustics. Cross sections for multiple imaging are derived.

Especially the singular isothermal ellipsoid provides a very convenient lens model, which is not much more complicated to handle than quasi-elliptical models, and we expect that the explicit equations derived here will be useful for future work.

Key words: gravitation – gravitational lensing

1. Introduction

Gravitational lenses with elliptical mass distribution have not been treated extensively in the literature. From the early work of Bourassa et al. (1973) and Bourassa & Kantowski (1975, see also Bray 1984), it became evident that even the calculation of the deflection angle from a lens with elliptical surface mass density is not trivial; the aforementioned authors introduced a complex formulation of lens theory to simplify the analytic treatment. Schramm (1990) calculated the deflection angle for elliptical mass distributions within the 'standard' vector formulation of lens theory; however, the resulting expressions for the components of the deflection angle are fairly complicated and can be used only for numerical work. For these reasons, lenses with elliptical surface mass densities have been used mainly for detailed numerical modelling of individual lens systems (see, e.g. Young et al. 1981a,b; Narasimha et al. 1982; Falco et al. 1991), except for an early statistical study (Bourassa & Kantowski 1976).

It is well known that the properties of lenses with axially-symmetric surface mass distributions ('symmetric lenses' henceforth) are qualitatively different from those with more realistic ('asymmetric') matter distributions (e.g. the degeneracy of the tangential caustic, see Schneider et al. 1992, hereafter SEF, Sect. 8.1). This means that the application of symmetric lens models can yield misleading results.

Faced with the dilemma that (easily treatable) symmetric lenses have non-generic properties and lenses with elliptical surface mass densities are difficult to investigate, a number of non-symmetric lens models were constructed whose properties resemble more or less those of elliptical lenses: (1) Symmetric lenses with external shear (Chang & Refsdal 1979,1984; Kovner 1987a; Kochanek 1991a); (2) Lenses with elliptical *potential* (Kovner 1987b,c; Blandford & Kochanek 1987; Kochanek & Blandford 1987; Kochanek et al. 1989); (3) Multipole expansions of elliptical lenses (Schneider & Weiss 1991; see also Kochanek 1991b). Fortunately, it turns out that all these models have the same general properties as elliptical lenses, and since they are much easier to handle, they have been used for modelling and statistical studies. Nevertheless, this approach has its drawbacks; for example, if the ellipticity in lenses with elliptical potentials becomes too large, the corresponding mass distributions obtain unphysical shapes.

In this paper we want to present a family of lens models with homoeoidal elliptical surface mass distributions. These models are a natural generalization of the isothermal sphere models widely used in lens theory, and are therefore termed 'isothermal

Send offprint requests to: P. Schneider

* Present address: Fraunhofer-Gesellschaft, Kreuzeckbahnstr. 19, D-82467 Garmisch-Partenkirchen, Germany

elliptical lenses'.[1] As we shall demonstrate, these lens models admit a fairly detailed analytical investigation. The deflection angle as a function of the impact vector of a light ray is given explicitly; simple expressions for the deflection angle, the Jacobian matrix, critical curves, caustics and cuts are obtained for the case with zero core size. For models with finite core size, the resulting expressions are more complicated; still, it is possible to obtain a full classification of these models in terms of their critical curves and caustics.

The rest of this paper is organized as follows: In Sect.2, we introduce our basic notation and the classes of lens models treated in this paper. Sections 3 and 4 provide analyses of models with vanishing and finite core radius, respectively.

After the work reported here had been completed, we learned that a similar project was undertaken by Kassiola & Kovner (1993). They also provided an analysis of elliptical isothermal lenses, with special emphasis on a comparison between elliptical matter distributions and elliptical potentials. In particular, they pointed out that elliptical potentials become completely unrealistic if the axis ratio becomes large, since the corresponding mass densities attain unphysical shapes. Our emphasis is directed more towards the critical structure of elliptical lenses. Where there is overlap between our papers, the results agree.

2. Gravitational lensing and isothermal galaxy models

2.1. Gravitational lensing

For gravitational lensing, we use the same notation as in SEF. Briefly, the lens equation reads

$$\boldsymbol{\eta} = \frac{D_\mathrm{s}}{D_\mathrm{d}}\boldsymbol{\xi} - D_\mathrm{ds}\hat{\boldsymbol{\alpha}}(\boldsymbol{\xi}) \quad , \tag{1}$$

where $\boldsymbol{\eta}$ denotes the source position, $\boldsymbol{\xi}$ the impact vector of the light ray in the lens plane, both measured with respect to an 'optical axis', $\hat{\boldsymbol{\alpha}}(\boldsymbol{\xi})$ is the deflection angle, related to the surface mass density $\Sigma(\boldsymbol{\xi})$ by

$$\hat{\boldsymbol{\alpha}}(\boldsymbol{\xi}) = \frac{4G}{c^2}\int_{\mathbf{R}^2}\Sigma(\boldsymbol{\xi}')\frac{\boldsymbol{\xi}-\boldsymbol{\xi}'}{|\boldsymbol{\xi}-\boldsymbol{\xi}'|^2}\,d^2\xi' \quad , \tag{2}$$

and $D_\mathrm{d}, D_\mathrm{s}, D_\mathrm{ds}$ denote the angular diameter distance to the lens, the source, and from the lens to the source, respectively.

The dimensionless lens equation is obtained by introducing a (conveniently chosen) length scale ξ_0 and defining

$$\begin{aligned} &\boldsymbol{x} = \frac{\boldsymbol{\xi}}{\xi_0} \quad , \quad \boldsymbol{y} = \frac{\boldsymbol{\eta}}{\eta_0} \quad \text{with} \quad \eta_0 = \frac{D_\mathrm{s}}{D_\mathrm{d}}\xi_0 \quad , \\ &\boldsymbol{\alpha}(\boldsymbol{x}) = \frac{D_\mathrm{d}D_\mathrm{ds}}{D_\mathrm{s}\xi_0}\hat{\boldsymbol{\alpha}}(\xi_0\boldsymbol{x}) = \frac{1}{\pi}\int_{\mathbf{R}^2}\kappa(\boldsymbol{x}')\frac{\boldsymbol{x}-\boldsymbol{x}'}{|\boldsymbol{x}-\boldsymbol{x}'|^2}\,d^2x' \quad , \\ &\text{with} \quad \kappa(\boldsymbol{x}) = \frac{\Sigma(\xi_0\boldsymbol{x})}{\Sigma_\mathrm{cr}} \quad , \quad \Sigma_\mathrm{cr} = \frac{c^2 D_\mathrm{s}}{4\pi G D_\mathrm{d} D_\mathrm{ds}} \quad , \end{aligned} \tag{3}$$

as

$$\boldsymbol{y} = \boldsymbol{x} - \boldsymbol{\alpha}(\boldsymbol{x}) \quad . \tag{4}$$

We also introduce the deflection potential

$$\psi(\boldsymbol{x}) = \frac{1}{\pi}\int_{\mathbf{R}^2}\kappa(\boldsymbol{x}')\ln|\boldsymbol{x}-\boldsymbol{x}'|\,\mathrm{d}^2x' \quad , \tag{5}$$

which is related to the deflection angle and the dimensionless surface mass density κ by

$$\boldsymbol{\alpha}(\boldsymbol{x}) = \nabla\psi(\boldsymbol{x}) \quad , \tag{6}$$

$$\nabla^2\psi = 2\kappa \quad , \tag{7}$$

and the Fermat potential

$$\Phi(\boldsymbol{x},\boldsymbol{y}) = \frac{1}{2}(\boldsymbol{x}-\boldsymbol{y})^2 - \psi(\boldsymbol{x}) \quad , \tag{8}$$

in terms of which the lens equation becomes

$$\nabla\Phi(\boldsymbol{x},\boldsymbol{y}) = 0 \quad , \tag{9}$$

where the gradient is to be taken with respect to $\boldsymbol{x}$.

The image distortion described by Eq.(4) is expressed in terms of the Jacobian matrix

$$A(\boldsymbol{x}) = \frac{\partial\boldsymbol{y}}{\partial\boldsymbol{x}} = \begin{pmatrix} 1-\kappa-\gamma_1 & -\gamma_2 \\ -\gamma_2 & 1-\kappa+\gamma_1 \end{pmatrix} \quad , \tag{10}$$

the second step being a decomposition into the local surface mass density $\kappa(\boldsymbol{x})$ (convergence) and the shear components

$$\gamma_1 = \frac{1}{2}(\psi_{,11} - \psi_{,22}) \quad , \tag{11a}$$

$$\gamma_2 = \psi_{,12} = \psi_{,21} \quad , \tag{11b}$$

$$\gamma = \sqrt{\gamma_1^2 + \gamma_2^2} \quad , \tag{11c}$$

where indices separated by a comma denote partial derivatives. The magnification $\mu(\boldsymbol{x})$ of an image (of an infinitesimally small source) at $\boldsymbol{x}$ is

$$\mu(\boldsymbol{x}) = \Big[\det A(\boldsymbol{x})\Big]^{-1} = \frac{1}{(1-\kappa)^2-\gamma^2} \quad . \tag{12}$$

The time delay between two images at $\boldsymbol{x}^{(1)}$ and $\boldsymbol{x}^{(2)}$ is given by

$$c\,\delta t = (1+z_\mathrm{d})\frac{D_\mathrm{s}\xi_0^2}{D_\mathrm{d}D_\mathrm{ds}}\Big[\Phi(\boldsymbol{x}^{(1)},\boldsymbol{y}) - \Phi(\boldsymbol{x}^{(2)},\boldsymbol{y})\Big] \quad . \tag{13}$$

[1] Throughout this paper, the term 'isothermal' should not imply a dynamical model for the mass distribution, but should merely indicate that the surface mass density asymptotically decreases as 1/(distance).

2.2. *Isothermal galaxy models for lensing*

If one considers a galaxy as a spherically-symmetric, self-gravitating concentration of stars behaving like an ideal gas in hydrostatic equilibrium, one obtains a differential equation for its radial mass distribution (Binney & Tremaine 1987, Eq.(4-115b)). One simple and analytic solution of this equation is called *singular isothermal sphere* (SIS). Its surface mass density, projected onto the lens plane, is given by

$$\Sigma(\boldsymbol{\xi}) = \frac{v^2}{2G}\frac{1}{\xi} \quad , \tag{14}$$

where v is the velocity dispersion along the line of sight. We have used polar coordinates $\boldsymbol{\xi} =: (\xi\cos\varphi, \xi\sin\varphi)$ in the lens plane. Choosing the length scale

$$\xi_0 := 4\pi\frac{v^2}{c^2}\frac{D_\mathrm{d}D_\mathrm{ds}}{D_\mathrm{s}} \tag{15}$$

and $x := \xi/\xi_0$, Eqs.(3) and (4) yield

$$\kappa(x) = \frac{1}{2x} \quad , \tag{16}$$

and the lens equation becomes

$$\boldsymbol{y} = \boldsymbol{x} - \frac{\boldsymbol{x}}{|\boldsymbol{x}|} \quad . \tag{17}$$

Due to the simplicity of this equation, the SIS is frequently used as gravitational lens model (e. g., Turner et al. 1984; see Sect. 8.1.4 of SEF). We mention in passing that this gravitational lens also fits to a simple disk model for spirals known as Mestel-disk (Mestel 1963), if the symmetry axis of the model is parallel to the optical axis.

Analytic solutions of the aforementioned differential equation without the central singularity are not known. In lens theory, a frequently used surface mass density for an 'isothermal' sphere with finite core radius ξ_c is

$$\Sigma(\boldsymbol{\xi}) = \frac{v^2}{2G}\frac{1}{\sqrt{\xi^2+\xi_\mathrm{c}^2}} = \frac{\Sigma_0}{\sqrt{1+\xi^2/\xi_\mathrm{c}^2}} \quad , \tag{18}$$

where $\Sigma_0 = v^2/(2G\xi_\mathrm{c})$ is the central surface mass density. The corresponding dimensionless surface mass density is obtained with the length scale (15), as

$$\kappa(\boldsymbol{x}) = \frac{1}{2\sqrt{x^2+x_\mathrm{c}^2}} \quad \text{with} \quad x_\mathrm{c} = \frac{\xi_\mathrm{c}}{\xi_0} \quad . \tag{19}$$

We shall term this lens model *nonsingular isothermal sphere* (NIS).

The generalizations of the isothermal sphere lens models to more realistic, elliptical lenses is now straightforward: we replace in Eqs. (14) and (18) the radial coordinate ξ by

$$\zeta := \sqrt{\xi_1^2 + f^2\xi_2^2} \quad , \tag{20}$$

which is constant on ellipses with minor axis ζ, major axis ζ/f, and thus axis ratio f. Hence, we define the surface mass density of the *singular isothermal ellipsoid* (SIE) to be

$$\Sigma(\boldsymbol{\xi}) = \frac{\sqrt{f}v^2}{2G}\frac{1}{\sqrt{\xi_1^2+f^2\xi_2^2}} = \frac{\sqrt{f}v^2}{2G}\frac{1}{\zeta} \quad , \tag{21a}$$

where the normalization is chosen such that the mass inside an elliptical iso-density contour for fixed Σ is independent of f. The value of the axis ratio f is taken from the interval $0 < f \leq 1$; in many of the calculations in Sects. 3 and 4, $f < 1$ is asumed, and the symmetric model is obtained in the limiting case $f \to 1$. Using the same length scale as in the symmetric case, Eq.(15), we find for the dimensionless surface mass density

$$\kappa(x,\varphi) = \frac{\sqrt{f}}{2x\Delta(\varphi)} = \frac{\sqrt{f}}{2b} \quad , \tag{21b}$$

where we have used the definitions

$$\Delta(\varphi) = \sqrt{\cos^2\varphi + f^2\sin^2\varphi} \quad , \tag{21c}$$

$$b = \frac{\zeta}{\xi_0} = x\Delta = \sqrt{x_1^2 + f^2x_2^2} \quad . \tag{21d}$$

Moreover, this corresponds to the surface mass density of a Mestel-disk with its symmetry axis non-parallel to the optical axis.

We generalize the NIS now in the same way as the singular models. Introducing again a core 'radius' ζ_c, with its dimensionless value being defined as $b_\mathrm{c} = \zeta_\mathrm{c}/\xi_0$, we obtain for the surface mass density

$$\Sigma(\zeta) = \frac{v^2}{2G}\frac{\sqrt{f}}{\sqrt{\zeta^2+\zeta_\mathrm{c}^2}} = \frac{\Sigma_0}{\sqrt{1+\zeta^2/\zeta_\mathrm{c}^2}} \tag{22a}$$

with $\Sigma_0 = \sqrt{f}v^2/(2G\zeta_\mathrm{c})$, i.e.

$$\kappa(b) = \frac{\sqrt{f}}{2\sqrt{b^2+b_\mathrm{c}^2}} \quad . \tag{22b}$$

The lens model described by this surface mass density will be called *non-singular isothermal ellipsoid* (NIE). It fulfills the same 'constant-mass' property as the singular model if we keep the core radius fixed.

Isothermal lenses have the further drawback of having infinite total mass. This problem can be cured if the mass density beyond some tidal 'radius' drops faster than ζ^{-2}. If this tidal 'radius' is much larger than the typical length scale ξ_0 where strong lensing occurs, this cut-off does not affect the strong lensing properties of the deflector. A possibility for such a cut-off has been outlined in Kassiola & Kovner (1993). An alternative to obtain elliptical lenses with finite mass has been employed by Bourassa & Kantowski (1975) and Narasimha et al. (1982); they considered an ellipsoid with sharp boundary.

3. The singular isothermal ellipsoid

In this section we discuss the properties of the SIE. This is a two-parameter family of lens models, where one of the parameters, the velocity dispersion, can be scaled out; thus, the only non-trivial parameter is the axis ratio f. For later purposes, we also define

$$f' = \sqrt{1-f^2} \quad . \tag{23}$$

3.1. Deflection potential and lens equation

Poisson's Eq. (7), written in polar coordinates

$$\frac{1}{x}\frac{\partial}{\partial x}\left(x\frac{\partial\psi}{\partial x}\right) + \frac{1}{x^2}\frac{\partial^2\psi}{\partial\varphi^2} = 2\kappa = \frac{\sqrt{f}}{x\Delta(\varphi)} \quad , \tag{24}$$

can be reduced to the ordinary differential equation

$$\tilde{\psi} + \frac{d^2\tilde{\psi}}{d\varphi^2} = \frac{\sqrt{f}}{\Delta(\varphi)} \tag{25}$$

by the ansatz $\psi(x,\varphi) =: x\tilde{\psi}(\varphi)$. This equation can be solved using Green's method. The resulting deflection potential[2] is

$$\psi(x,\varphi) = \frac{\sqrt{f}x}{f'} \times \left[\sin\varphi \operatorname{arcsin}(f'\sin\varphi) + \cos\varphi \operatorname{arsinh}\left(\frac{f'}{f}\cos\varphi\right)\right] \tag{26a}$$

$$= \frac{\sqrt{f}x}{f'}\left[|\sin\varphi| \arccos\Delta + |\cos\varphi| \operatorname{arcosh}\frac{\Delta}{f}\right] \quad . \tag{26b}$$

$\tilde{\psi}$ describes the deviation of the deflection potential from that of the SIS, the latter being $\psi(x) = x$. Figure 1 shows a curve of constant ψ.

The gradient $\boldsymbol{\alpha} = \nabla\psi$ yields the deflection angle and the lens equation

$$\boldsymbol{y} = \boldsymbol{x} - \frac{\sqrt{f}}{f'}\left[\operatorname{arsinh}\left(\frac{f'}{f}\cos\varphi\right)\boldsymbol{e}_1 + \arcsin(f'\sin\varphi)\,\boldsymbol{e}_2\right] \tag{27a}$$

$$= \boldsymbol{x} - \frac{\sqrt{f}}{f'} \times \left[\operatorname{sgn}(\cos\varphi)\operatorname{arcosh}\frac{\Delta}{f}\boldsymbol{e}_1 + \operatorname{sgn}(\sin\varphi)\arccos\Delta\,\boldsymbol{e}_2\right] \tag{27b}$$

of the SIE, where $\boldsymbol{e}_i$ is the unit vector in the direction of x_i. Because of

$$\lim_{f\to 1}\left[\frac{\sqrt{f}}{f'}\operatorname{arsinh}\left(\frac{f'}{f}\cos\varphi\right)\right] = \cos\varphi \quad , \tag{28a}$$

$$\lim_{f\to 1}\left[\frac{\sqrt{f}}{f'}\arcsin(f'\sin\varphi)\right] = \sin\varphi \quad , \tag{28b}$$

the deflection angle of the SIE tends to that of the SIS in the limit $f \to 1$.

[2] It is indeed the correct physical solution of Eq.(7), since the deflection angle (27a) is equal to that obtained from (5) and (6), as will be shown in App.B.

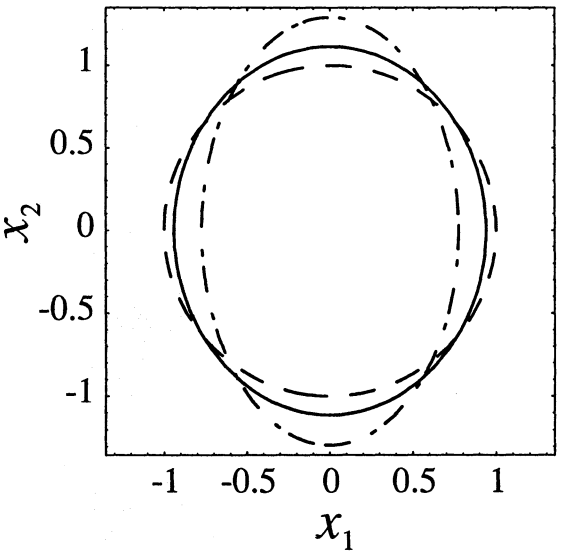

Fig. 1. Iso-density contours for the SIS (dashed curve) and the SIE (dash-dotted line) with $f = 0.6$, for the same value of κ in both cases. Also plotted is a curve of constant deflection potential ψ (solid curve), which is much rounder than the corresponding iso-density contour

3.2. Magnification, critical curve, cut and caustic

Differentiation of the lens equation yields the distortion matrix $A = \partial\boldsymbol{y}/\partial\boldsymbol{x}$. As a function of κ and φ, it reads

$$A = \begin{pmatrix} 1-2\kappa\sin^2\varphi & \kappa\sin(2\varphi) \\ \kappa\sin(2\varphi) & 1-2\kappa\cos^2\varphi \end{pmatrix} \quad . \tag{29}$$

It is somewhat surprising that this equation is formally identical to the corresponding equation for the SIS. As a consequence, the expressions for the magnification, $\mu = 1/\det A = 1/(1-2\kappa)$, and the trace of A, $\operatorname{tr}A = 1 + \det A$, are also formally identical for both, SIE and SIS. The components of the shear are $\gamma_1 = -\kappa\cos(2\varphi)$ and $\gamma_2 = -\kappa\sin(2\varphi)$.

As in the case of the SIS, due to the singularity of the surface mass density at the center of the lens, we find a region in the source plane where multiple images exist, but which is not enclosed by a caustic. According to Kovner (1987a), we call the curve surrounding this region the *cut*. If we remove the singularity by introducing a finite core radius (to be done in the next section), the cut will transform into a caustic. Therefore, a cut is the 'limiting case' of a caustic for vanishing core radius. Sources on the cut have an 'infinitely faint' image at the position of the mass singularity, i.e. at the origin of the lens plane. This splits into two images with the typical behaviour at critical curves once we introduce a finite core radius. Mathematically, the cut is therefore given by

$$\boldsymbol{y}(\varphi) = \lim_{x\to 0}\boldsymbol{y}(x,\varphi) = -\boldsymbol{\alpha}(\varphi) = -\frac{\sqrt{f}}{f'}\left[\operatorname{arsinh}\left(\frac{f'}{f}\cos\varphi\right)\boldsymbol{e}_1 + \arcsin(f'\sin\varphi)\,\boldsymbol{e}_2\right] \quad . \tag{30}$$

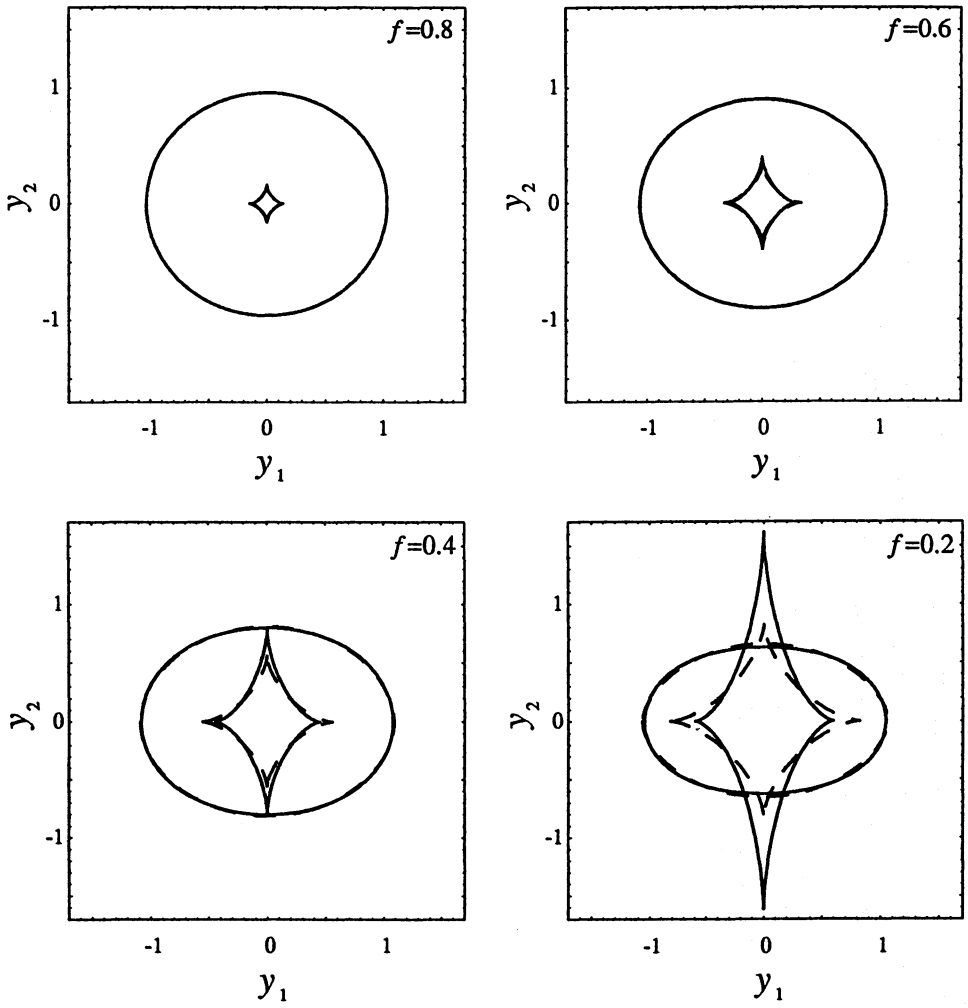

Fig. 2. Cut and caustic of the SIE. The caustic shows cusps on the axes. The dashed lines give cut and caustic of a different lens model called SIE-M1. This model will be described later in this section

The critical curve is given by $\det A(\boldsymbol{x}) = 0$ or $\kappa = 1/2$, or $x = \sqrt{f}/\Delta(\varphi)$. Inserting this equation into the lens Eq. (27a), we obtain a parametrized equation for the caustic,

$$y_1 = \frac{\sqrt{f}}{\Delta}\cos\varphi - \frac{\sqrt{f}}{f'}\operatorname{arsinh}\left(\frac{f'}{f}\cos\varphi\right) \quad , \tag{31a}$$

$$y_2 = \frac{\sqrt{f}}{\Delta}\sin\varphi - \frac{\sqrt{f}}{f'}\arcsin(f'\sin\varphi) \quad . \tag{31b}$$

Hence, in contrast to the SIS, the caustic of the SIE does not degenerate into a point. Figure 2 shows cuts and caustics for different axis ratios.

Next, we calculate the intersections of cut and caustic with the axes. For the cut, we obtain

$$y_1 = \pm s_1 \quad \text{with} \quad s_1 := \frac{\sqrt{f}}{f'}\operatorname{arcosh}\frac{1}{f} \quad , \tag{32a}$$

$$y_2 = \pm s_2 \quad \text{with} \quad s_2 := \frac{\sqrt{f}}{f'}\arccos f \quad . \tag{32b}$$

The intersections of the caustic with the axes, i.e. the positions of the cusps, are given by

$$y_1 = \pm\left(s_1 - \sqrt{f}\right) \quad , \tag{33a}$$

$$y_2 = \mp\left(s_2 - \frac{1}{\sqrt{f}}\right) \quad . \tag{33b}$$

The upper signs in these equations refer to those points of the critical curve which are on the positive half-axes. We can see that the cusps on the 1-axis always fall within the region surrounded by the cut. The cusps on the 2-axis are inside (outside) the cut if $f > f_0$ ($f < f_0$), where f_0 is the solution of the equation $2f_0 \arccos f_0 = \sqrt{1 - f_0^2}$. Numerically, $f_0 = 0.3942\ldots$. Images with given magnification μ lie on ellipses with $x = \sqrt{f}\mu/[(\mu - 1)\Delta]$.

3.3. Solution of the lens equation

It appears impossible to invert the lens equation of the SIE analytically. We can only describe a (simple) procedure for finding the images of a given source position. There is no need for numerical methods like the grid-search algorithm, since the lens equation can be reduced to a one-dimensional equation: If we multiply the first component of the lens Eq. (27a) with $\cos\varphi$ and the second with $\sin\varphi$, we find for the radial coordinate

$$x = y_1\cos\varphi + y_2\sin\varphi + \tilde{\psi}(\varphi) \quad . \tag{34}$$

This is reinserted into the lens equation to obtain a one-dimensional, implicit equation for φ,

$$\left[y_1 + \frac{\sqrt{f}}{f'}\operatorname{arsinh}\left(\frac{f'}{f}\cos\varphi\right)\right]\sin\varphi - \left[y_2 + \frac{\sqrt{f}}{f'}\arcsin(f'\sin\varphi)\right]\cos\varphi = 0 \quad . \tag{35}$$

This equation can now be solved with root-finding-algorithms. For a source 'outside' of the cut, this equation produces a spurious image (the second image, for an explanation see below), which must be dropped.

In the special case of a source on the positive 1-axis, we can find an image with $\varphi = 0$ and $x = y_1 + s_1$. For $y_1 < s_1$, i.e. a source inside the region surrounded by the cut, we find a second image at $\varphi = \pi$ and $x = s_1 - y_1$. If the source lies also 'within' the caustic, there are two further images away from the axes. These image positions can only be found by solving the implicit Eq. (35). The situation is identical for the 2-axis. We only have to replace 0 by $\pi/2$, π by $3\pi/2$ and s_1 and y_1 by s_2 and y_2, respectively.

3.4. Image positions and numbers

In this paragraph we want to describe qualitatively the image positions, numbers, and some other properties for given sources. Due to the symmetry of the lens, we can restrict the treatment to sources in the first quadrant. We will move source positions from 'far outside' to the origin of the source plane, i.e. behind the center of the SIE. Moreover, we assume to cross the cut first and then the caustic. We treat the other case later, which can occur only for $f < f_0$.

A source in the 'outer' region has only one image, which is in the first quadrant of the lens plane. This 'first image' has positive parity and small magnification $\mu \gtrsim 1$. Independently of the source position it is always within the first quadrant and stays 'outside' the critical curve; hence, its parity stays positive. If the source crosses the cut, a 'second image' appears in the third quadrant very close to the lens center. Since $\mu = 1/(1-2\kappa)$, it is very faint. At the crossing, the first image is magnified by a factor of approximately two. The second image is always found within the critical curve, and its parity is negative. The even number of images is due to the mass singularity.

Crossing the caustic, we will find two new 'critical images' in the second quadrant. Of course, one of it lies 'within' the critical curve, having negative parity, and the second one is 'outside' with positive parity. The absolute value of the magnification is very high due to the properties of fold singularities, but decreases rapidly when we move the source towards the origin.

In the special case of a source at the origin of the source plane, we find four images on the axes of the lens plane at $x_1 = \pm s_1$ and $x_2 = \pm s_2$. The images with negative parity – the second image and one of the critical images – lie within the region enclosed by the critical curve and on the 2-axis. The others are outside the critical curve, on the 1-axis.

Obviously the second image and the critical images appear in opposite sequence, if the source crosses the caustic first and the cut afterwards. Having a source in one of the other three quadrants, we must interchange the image positions according to the symmetry of the lens model.

3.5. Large magnification, time delay and cross sections

A source close to, but inside a caustic curve has two images close to, and on opposite sides of the corresponding critical curve. The universality of the lens mapping close to fold singularities (e.g. Blandford & Narayan 1986) allows one to obtain simple relations between the magnifications of the images, their separation and their time delay. After some tedious, but straightforward algebra, one obtains for the magnification by applying Eq. (6.20) of SEF to the SIE

$$|\mu| = \frac{4\sqrt{f}\Delta}{f'^2|\sin(2\varphi)|}\frac{1}{\delta x} \quad , \tag{36}$$

and for the time delay δt – from Eq. (6.21a) of SEF

$$c\,\delta t = 2\pi^2(1+z_\mathrm{d})\frac{v^4}{c^4}\frac{D_\mathrm{d}D_\mathrm{ds}}{D_\mathrm{s}}\frac{f'^2|\sin(2\varphi)|}{\sqrt{f}\Delta}(\delta x)^3 \quad , \tag{37}$$

where δx is the separation of the images in the dimensionless units. Interestingly, both relations are ill-behaved in the limit $f \to 1$ (i.e. $f' \to 0$); this is due to the fact that these relations have been derived for a generic fold singularity. For the spherical case $f = 1$, this singularity degenerates into a point, and the universality relations break down. Also note that both relations behave peculiarly for $\varphi = 0, \pi/2, \pi, 3\pi/2$; there, the source is near a cusp singularity, and again the universality relations for a fold break down. If we insert typical values into these formulae, e.g. $v = 220$km/s, $z_\mathrm{d} = 0.5$ and $z_\mathrm{s} = 2$ in an Einstein-de Sitter universe with Hubble constant $H_0 = 100h$ km/(s Mpc), and a SIE with $f = 0.8$ at $\varphi = \pi/4$, we obtain the approximate relations

$$|\mu| \simeq \frac{7''.2}{\delta\theta} \quad , \tag{38a}$$

$$\delta t \simeq \frac{15\mathrm{h}}{h}\left(\frac{\delta\theta}{0''.8}\right)^3 \quad ; \tag{38b}$$

$\delta\theta$ denotes the angular separation between the images. Hence, two images with a magnification $|\mu| = 20$ have an angular separation of about $0''.36$ and a time delay of roughly three hours ($h = 0.5$).

We consider next some lensing cross sections. Briefly, a (dimensionless) cross section σ is related to the physical area in the source plane $\hat{\sigma}$ via $\hat{\sigma} = \eta_0^2\sigma$ – for an introduction into the concept of cross sections see SEF, Sect. 11.1.

Again due to the universality of the lens mapping near fold and cusp singularities, the cross section $\sigma(\mu_\mathrm{p} \geq \mu)$ for a point source to be magnified by more than μ (for $\mu \to \infty$) follows a

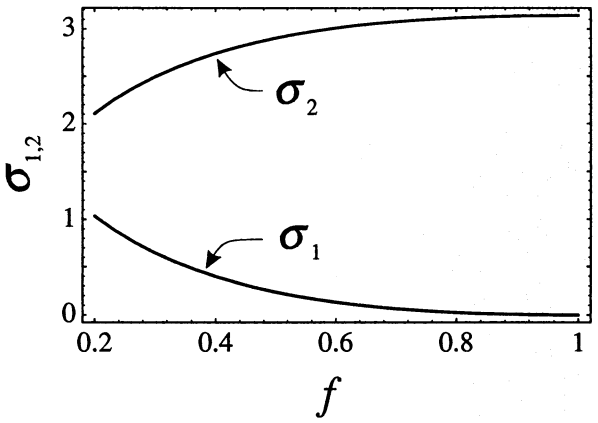

Fig. 3. Cross sections of the cut (σ_2) and the caustic (σ_1) for the SIE. The cut and caustic cross sections are identical to the two- and four-image cross sections, if $f > f_0$

simple relation (Blandford & Narayan 1986; Mao 1992; Schneider & Weiss 1992). Applying Eqs. (11.21) and (11.22) of SEF to the SIE, we find

$$\sigma(\mu_p > \mu) = \frac{4\pi}{\mu^2} + \frac{16\sqrt{6}}{15}\frac{1+f}{f'}\frac{1}{\mu^{5/2}} \quad . \tag{39}$$

Interestingly, the μ^{-2}-component (the contribution from folds and the inside of cusps) is *independent* of f. On the other hand, the $\mu^{-5/2}$-component (the component from the outside of cusps) diverges for $f \to 1$, since in this limit, the whole caustic (including the cusps) degenerates. This does not imply that σ diverges for fixed μ and $f \to 1$; it just means that the value of μ, beyond which the cusp contribution in Eq.(39) is a good approximation, diverges as $f \to 1$.

The area enclosed by either cut or caustic can be calculated as

$$\sigma = 4f \int_f^1 y_2(\Delta)\left|\frac{dy_1}{d\Delta}\right| d\Delta \quad , \tag{40}$$

due to the symmetry of the lens model. Inserting Eqs. (31) and (32), we find in turn for the area enclosed by the caustic

$$\sigma_1 = \frac{4f}{f'^2}\int_f^1 \left(\frac{\sqrt{1-\Delta^2}}{\Delta} - \arccos\Delta\right)\frac{\sqrt{\Delta^2 - f^2}}{\Delta^2}\, d\Delta \tag{41}$$

and the area enclosed by the cut

$$\sigma_2 = \frac{4f}{f'^2}\int_f^1 \frac{\arccos\Delta}{\sqrt{\Delta^2 - f^2}}\, d\Delta \quad , \tag{42}$$

which are shown in Fig. 3. For $f > f_0$, σ_1 and σ_2 are the cross sections for four and two images, respectively.

3.6. Multipole expansion

We can also use the multipole expansion developed by Schneider & Weiss (1991) to approximate the elliptical mass distribution of the SIE. In this paragraph we want to consider the multipole expansion up to the quadrupole term. In principle it is possible to treat the whole expansion analytically, though it becomes very cumbersome to find the expansion coefficients. We summarize only some interesting results without giving details.

The surface mass density of the SIE-M1, as we call this lens model, is given by

$$\kappa(x,\varphi) = \frac{1}{2x}\Big[k + 3a\cos(2\varphi)\Big] \quad , \tag{43}$$

where we have used the definitions

$$k(f) := \frac{2\sqrt{f}K'}{\pi} \quad , \tag{44a}$$

$$a(f) := \frac{4\sqrt{f}}{3\pi f'^2}\Big[2E' - (1+f^2)K'\Big] \quad ; \tag{44b}$$

$E' \equiv E(f')$ and $K' \equiv K(f')$ are the complete elliptical integrals of the first and the second kind as defined by Gradshteyn & Ryzhik (1980), Eqs. (8.112).

Typical for the expansion up to the quadrupole term is the dumbbell-shaped distortion of the originally elliptical mass distribution shown in Fig. 4.

The deflection potential is given by

$$\psi(x,\varphi) = kx - ax\cos(2\varphi) \quad ; \tag{45}$$

the lens equation reads

$$y_1 = (x + 3a - k)\cos\varphi - 2a\cos^3\varphi \quad , \tag{46a}$$

$$y_2 = (x - 3a - k)\sin\varphi + 2a\sin^3\varphi \quad . \tag{46b}$$

We find for the distortion matrix

$$A = \begin{pmatrix} 1 - 2\kappa\sin^2\varphi & \kappa\sin(2\varphi) \\ \kappa\sin(2\varphi) & 1 - 2\kappa\cos^2\varphi \end{pmatrix} \quad . \tag{47}$$

Hence, the expressions for the magnification, the shear and the trace of A can be adopted from the SIE. We note here in passing that the validity of these equations can be shown by induction for every order of expansion. The critical curve is parametrized by the equation

$$x = k + 3a\cos(2\varphi) \quad , \tag{48}$$

the corresponding caustic is given by

$$y_1 = 4a\cos^3\varphi \quad , \tag{49a}$$

$$y_2 = -4a\sin^3\varphi \quad , \tag{49b}$$

or

$$y_2 = \pm\Big[(4a)^{2/3} - y_1^{2/3}\Big]^{3/2} \quad . \tag{50}$$

The cut of the SIE-M1 reads

$$y_1 = (3a - k)\cos\varphi - 2a\cos^3\varphi \quad , \tag{51a}$$

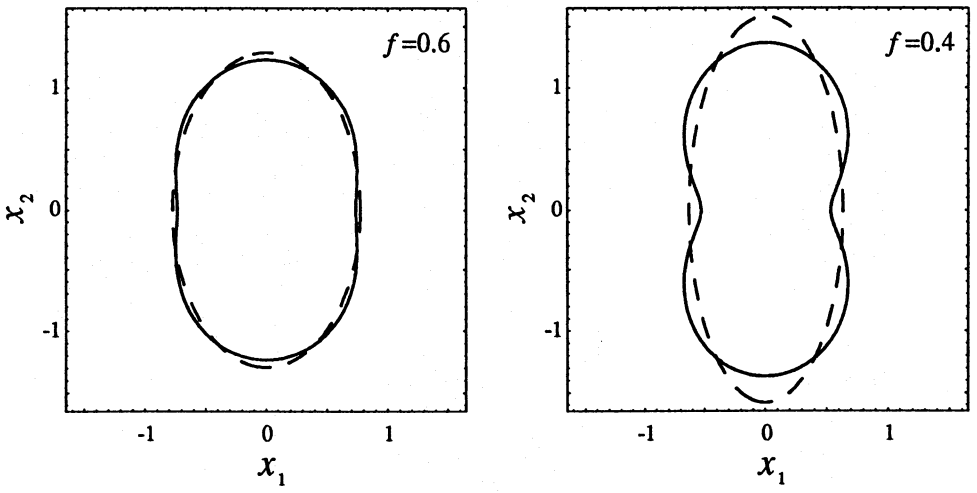

Fig. 4. Iso-density contours $\kappa = 1/2$ for the SIE-M1. The dashed lines are the corresponding iso-density contours for the SIE. Due to the expressions for the magnification given in the text, these lines coincide with the critical curves for both lens models

$$y_2 = (-3a - k)\sin\varphi + 2a\sin^3\varphi \quad . \tag{51b}$$

Cut and caustic of the SIE-M1 are plotted in Fig. 2 as dashed lines for a comparison with those of the SIE.

The lens equation of the SIE-M1 is easier to solve than for the SIE, because we are left with a polynomial in $\cos\varphi =: t$, namely

$$16a^2t^4 - 8ay_1t^3 + \left(|\boldsymbol{y}|^2 - 16a^2\right)t^2 + 8ay_1t - y_1^2 = 0 \quad . \tag{52}$$

The x-component is given by

$$x = y_1\cos\varphi + y_2\sin\varphi + k - a\cos(2\varphi) \quad . \tag{53}$$

The cross sections for caustic and cut are

$$\sigma_1 = 6\pi a^2 \quad , \tag{54}$$

$$\sigma_2 = \frac{1}{2}\pi\left(2k^2 - 3a^2\right) \quad . \tag{55}$$

4. Nonsingular isothermal lens models

Now we want to discuss the mathematical properties of non-singular isothermal lens models. In the case of a symmetric lens it is possible to obtain analytic results for a very general class of lens models. This is, for example, done in SEF, Sect. 8.1. But since the lens model which we call non-singular isothermal sphere (NIS) is not well-known, we summarize some properties of this model in the first part of this section. In the second part we generalize again the symmetric lens to the non-singular isothermal ellipsoid (NIE).

4.1. The nonsingular isothermal sphere

The surface mass density of the NIS is given by Eq.(19). The lens equation becomes one-dimensional in this case. With $\boldsymbol{y} = \boldsymbol{e}_y y$ and $\boldsymbol{x} = \boldsymbol{e}_y x$ ($\boldsymbol{e}_y := \boldsymbol{y}/|\boldsymbol{y}|$), the deflection angle is

$$\alpha(x) = \frac{1}{x}\sqrt{x^2 + x_c^2} - \frac{x_c}{x} = \frac{m(x)}{x} \quad , \tag{56}$$

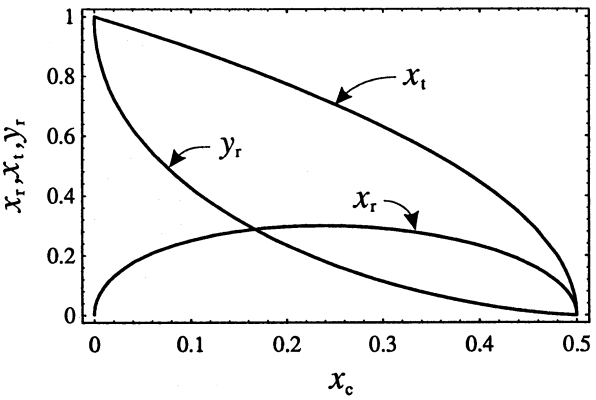

Fig. 5. The radii of the critical curves of the NIS and the radius of the radial caustic y_r as a function of the core radius

where we have used the dimensionless 'mass'

$$m(x) = 2\int_0^x x'\kappa(x')\,dx' = \sqrt{x^2 + x_c^2} - x_c \quad . \tag{57}$$

Note that x can become negative in these equations. The deflection potential is given by

$$\psi(x) = \sqrt{x^2 + x_c^2} - x_c\ln\left(x_c + \sqrt{x^2 + x_c^2}\right) \tag{58a}$$

$$= \sqrt{x^2 + x_c^2} - x_c\,\mathrm{arsinh}\frac{x_c}{|x|} - x_c\ln|x| \quad , \tag{58b}$$

which is found by integration of the deflection angle.

There are two different critical curves, called radial and tangential critical curves, provided $x_c < 1/2$ (for a detailed discussion see SEF, Sect. 8.1). The radius of the radial critical curve is given by $dy/dx = 0$, or

$$x_r^2 = \frac{1}{2}\left(2x_c - x_c^2 - x_c\sqrt{x_c^2 + 4x_c}\right) \quad . \tag{59}$$

The lens equation can be reduced to a third order polynomial equation in x, namely

$$x^3 - 2yx^2 + \left(y^2 - 1 + 2x_c\right)x - 2x_cy = 0 \quad . \tag{60}$$

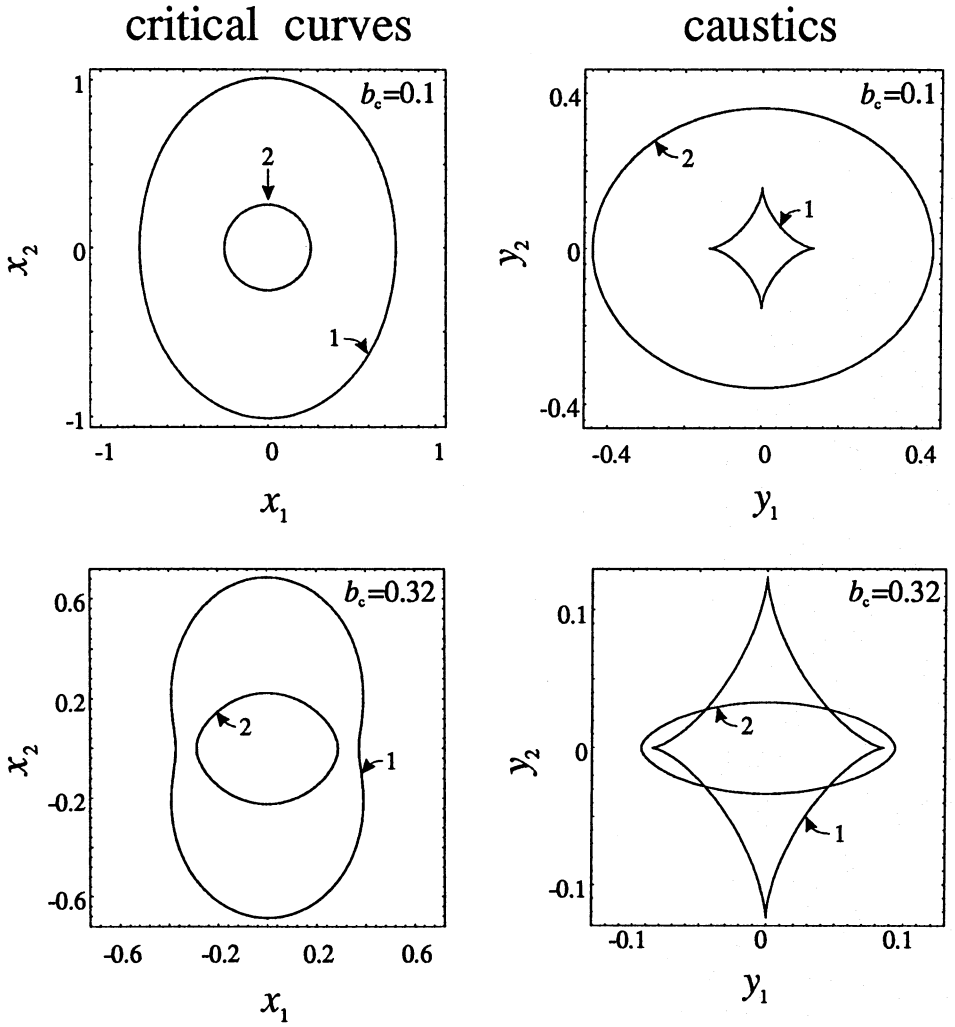

Fig. 6. Critical curves and caustics for the NIE with $f = 0.8$. In this figure, we have $b_c < f^{3/2}/2$, meaning that both critical curves and their caustics exist. The numbers in the figure correspond to the notation in the text

The radius of the tangential critical curve which maps into a point at $y = 0$ is found by solving this polynomial for $y = 0$, giving

$$x_t = \sqrt{1 - 2x_c} \quad . \tag{61}$$

Figure 5 shows the dependency of x_r, x_t and the radius of the radial caustic y_r on the core radius.

4.2. The nonsingular isothermal ellipsoid

4.2.1. Lens equation

The lens equation of the NIE, with surface mass density (22b), is found by using the complex representation of lens theory together with the results of Bourassa & Kantowski (1975) and Bray (1984). Their results are summarized in App.A , whereas the detailed calculations are given in App.B. Splitting the complex deflection angle into its real and imaginary parts, we obtain for the lens equation

$$y_1 = x_1 - \frac{\sqrt{f}}{4f'} \ln \frac{Q_+}{Q_-} \quad , \tag{62a}$$

$$y_2 = x_2 + \frac{\sqrt{f}}{2f'}(\arg R - \arg S) \quad , \tag{62b}$$

with

$$Q_\pm := \frac{\left(f'\sqrt{b^2 + b_c^2} \pm x_1\right)^2 + f^4 x_2^2}{(fx^2 \pm f' b_c x_1)^2 + f'^2 b_c^2 x_2^2} \quad , \tag{62c}$$

$$R := x_1^2 + f^4 x_2^2 - f'^2\left(b^2 + b_c^2\right) - 2\mathrm{i} f^2 f' \sqrt{b^2 + b_c^2}\, x_2 \quad , \tag{62d}$$

$$S := f^2 x^2 - f'^2 b_c^2 - 2\mathrm{i} f f' b_c x_2 \quad . \tag{62e}$$

Of course, for $b_c = 0$, these equations reduce to the lens equation of the SIE.

The complicated deflection angle causes strong limitations on an analytic treatment of this model, but it is possible to find the critical curves and the caustic structures without numerical methods. This will be done below.

4.2.2. Shear

As for the lens equation, we can split the complex shear leading to

$$\gamma_1 = \left[f^2\left(x_1^2 - x_2^2\right) - f'^2 b_c^2\right] P \quad , \tag{63a}$$

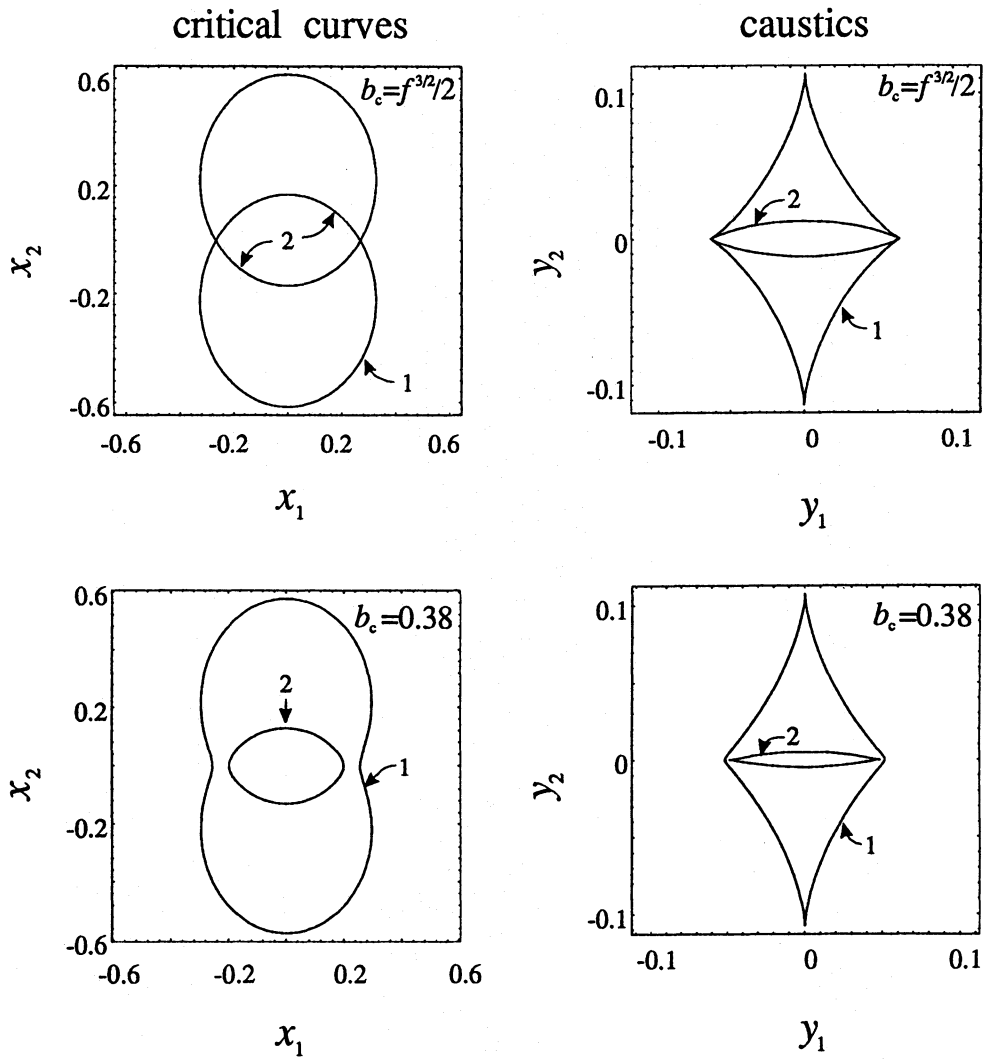

Fig. 7. Critical curves and caustics of the NIE with $f = 0.8$. The condition $b_c = f^{3/2}/2$ is fulfilled in the upper panels. This means that the caustics show an hyperbolic umbilic. Here also $b_c < f^{3/2}/(1+f)$ – so both critical curves and caustics exist

$$\gamma_2 = 2f^2 x_1 x_2 P \quad , \tag{63b}$$

with

$$P := \frac{\sqrt{f}}{f^4x^4 - 2f^2f'^2b_c^2\left(x_1^2 - x_2^2\right) + f'^4b_c^4} \times \\ \times \left[\frac{\kappa}{\sqrt{f}}\left(x_1^2 + f^4x_2^2\right) - \frac{1+f^2}{2}\sqrt{b^2+b_c^2} + fb_c\right] \quad . \tag{63c}$$

These expressions become much simpler if we use κ as independent variable and restrict the treatment to the axes of the coordinate system. We obtain on the positive 1-axis

$$\gamma_1 = \kappa - \frac{2f^{3/2}\kappa}{f^{3/2} + 2b_c\kappa} \quad , \quad \gamma_2 = 0 \quad , \tag{64a}$$

and on the positive 2-axis

$$\gamma_1 = \frac{2\kappa}{1 + 2b_c\sqrt{f}\kappa} - \kappa \quad , \quad \gamma_2 = 0 \quad . \tag{64b}$$

4.2.3. Critical curves and caustics

Equations (64) are very helpful for studying the behaviour of the critical curves and the caustics of the NIE. We solve the equation $D = (1-\kappa)^2 - \gamma^2 = 0$ in terms of κ to obtain the intersections of the critical curves with the axes. For the 1-axis, we end up with a third-order polynomial in κ_1 (the index '1' indicates that we are dealing with the intersections between the caustics and the 1-axis), which can be factorized,

$$D\left(f^{3/2} + 2b_c\kappa_1\right)^2 \\ = \left(f^{3/2} + 2b_c\kappa_1 - 2f^{3/2}\kappa_1\right)\left(f^{3/2} + 2b_c\kappa_1 - 4b_c\kappa_1^2\right) \quad . \tag{65}$$

The positive roots of the equation $D = 0$ are

$$\kappa_{1,1} = \frac{f^{3/2}}{2(f^{3/2} - b_c)} \quad , \tag{66a}$$

$$\kappa_{1,2} = \frac{1}{4}\left(1 + \sqrt{1 + \frac{4f^{3/2}}{b_c}}\right) \quad . \tag{66b}$$

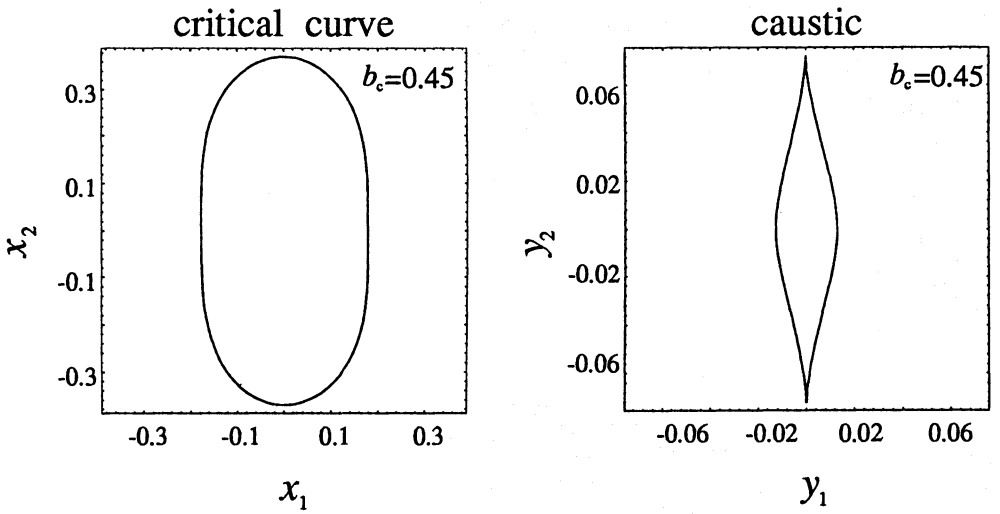

Fig. 8. Exterior critical curve and first caustic for the NIE with $f = 0.8$. Due to the fact that the core radius lies now between $f^{3/2}/(1+f)$ and $\sqrt{f}/(1+f)$, we get only one critical curve

The same can be done on the 2-axis, yielding

$$D\left(1+2\sqrt{f}b_c\kappa_2\right)^2 = \left(1+2b_c\sqrt{f}\kappa_2-2\kappa_2\right)\left(1+2b_c\sqrt{f}\kappa_2-4b_c\sqrt{f}\kappa_2^2\right) \quad (67)$$

and

$$\kappa_{2,1} = \frac{1}{2\left(1-b_c\sqrt{f}\right)} \quad , \quad (68a)$$

$$\kappa_{2,2} = \frac{1}{4}\left(1+\sqrt{1+\frac{4}{b_c\sqrt{f}}}\right) \quad . \quad (68b)$$

The two solutions indicate that the NIE will have two independent critical curves. This is what we expect from the singular case, since the removal of the singularity transforms the cut to an ordinary caustic, yielding a second critical curve. To see whether the caustics have fold or cusp catastrophes on the axes, we map tangent vectors $\boldsymbol{T}$ of the critical curve to the source plane via $A \cdot \boldsymbol{T}$, using Eqs.(64). Due to the symmetry of the problem, we have $\boldsymbol{T} \propto (0,1)$ on the 1-axis and $\boldsymbol{T} \propto (1,0)$ on the 2-axis. $A \cdot \boldsymbol{T}$ vanishes at the positions given by $\kappa_{i,1}, i = 1,2$, and is non-zero for the other cases. Since $A \cdot \boldsymbol{T}$ is a necessary condition for a cusp, the solutions $\kappa_{i,2}, i = 1,2$, must correspond to a fold. Excluding the case $\kappa_{i,1} = 1, i = 1,2$, which can only occur on the 1-axis, we find that these caustic points correspond to cusps.

If we consider a very small core, we can achieve better insight into the shapes of the critical curves and the caustics using the results from the singular case. We find $\lim_{b_c \to 0} \kappa_{i,1} = 1/2$, meaning that these points tend to the critical curve of the SIS. This means that the points given by $\kappa_{i,1}$ are connected by one critical curve, and due to $\kappa_{i,1} < \kappa_{i,2}$ (for small core radii), this curve encloses the other one. Therefore we call it *exterior* or *first critical curve* and the caustic *first caustic*. This caustic must have four cusps on the axes due to the behaviour in the singular case and $A \cdot \boldsymbol{T} = 0$. It also corresponds to the tangential critical curve in the limiting case of rotational symmetry. On the other hand, we find $\lim_{b_c \to 0} \kappa_{i,2} = \infty$, meaning that this critical curve contracts into the lens center, and showing that the caustic transforms into the cut. We call these structures *interior* or *second critical curve* and *second caustic*.

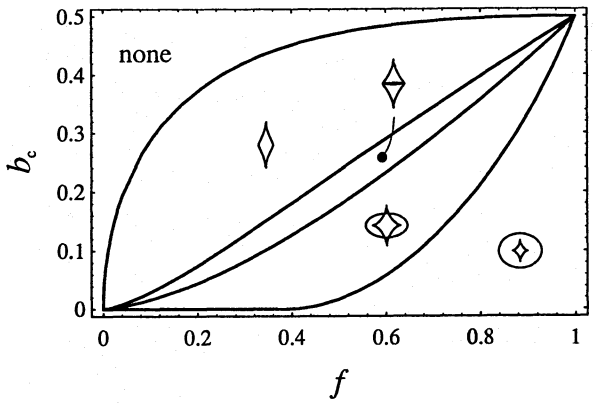

Fig. 9. The different topologies of the caustics in dependence of f and b_c

Now we increase the core radius. The first special case occurs when $\kappa_{1,1} = \kappa_{1,2} = 1$. Because of Eqs.(66), this implies $b_c = f^{3/2}/2$. Since the distortion matrix vanishes totally in this case, the caustics now show a hyperbolic umbilic on the 1-axis (for a discussion of these catastrophes see SEF, Sect. 6.3). Due to the properties of a hyperbolic umbilic, the two cusps on the 1-axis are passed to the other caustic, yielding two caustics with two cusps each for $b_c > f^{3/2}/2$. In other words, the rôles of $\kappa_{1,i}; i = 1,2$ are interchanged. The point corresponding to $\kappa_{1,1}$ is now connected to $\kappa_{2,2}$, since now $\kappa_{1,1} > \kappa_{1,2}$.

Since $\kappa \leq \kappa(0)$, Eq.(22b) implies $\kappa \leq \sqrt{f}/(2b_c)$. For the values $\kappa_{1,1}$ and $\kappa_{2,2}$, we obtain the condition $b_c < f^{3/2}/(1+f)$. Therefore, the second critical curve and the second caustic exist

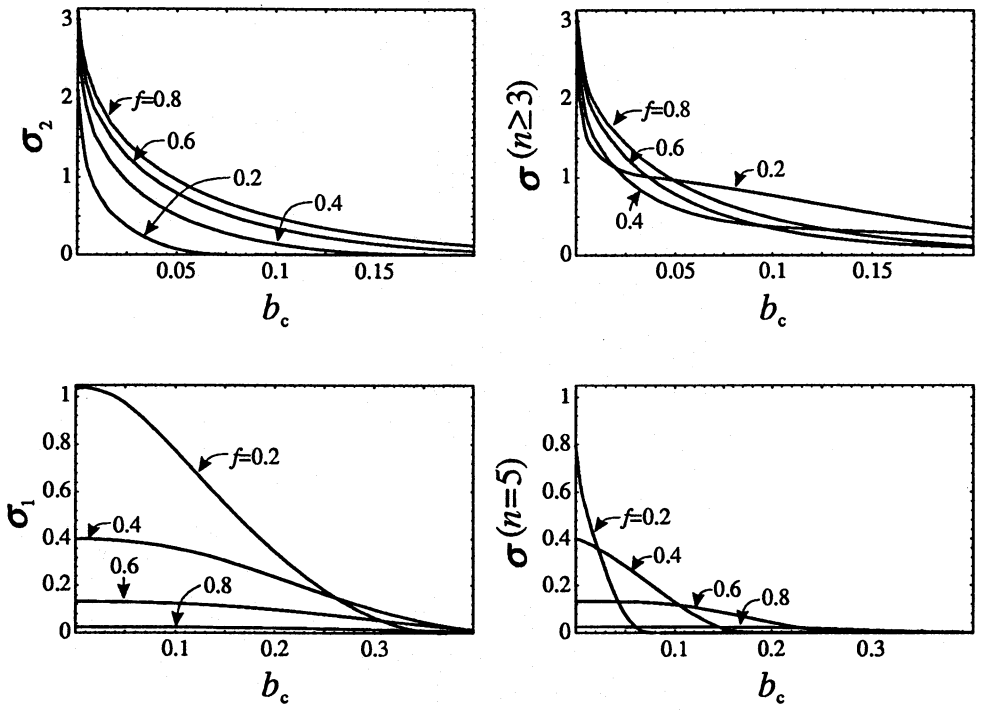

Fig. 10. Cross sections for the NIE. The plots on the left side show the cross section of the second and the first caustic, the ones on the right the cross sections for multiple imaging and for five images

only if this condition is fulfilled. For the existence of the other critical curve and caustic, we require $b_c < \sqrt{f}/(1+f)$.

We can find the complete critical curves and caustics without numerical methods. The equation $D = 0$ is equivalent to

$$8c_3\kappa^3 + 4c_2\kappa^2 + 2c_1\kappa + c_0 = 0 \quad , \tag{69a}$$

with the coefficients

$$c_3 := \left(b_c f^{3/2} - b_c^2 - b_c^2 f^2\right)\Delta^2 + 8b_c^2 f^2 \quad , \tag{69b}$$

$$c_2 := \left(-2b_c f^{3/2} + b_c^2 + b_c^2 f^2\right)\Delta^2 - 4b_c^2 f^2 \quad , \tag{69c}$$

$$c_1 := 2b_c f^{3/2}\Delta^2 - f^3 \quad , \tag{69d}$$

$$c_0 := f^3 \quad . \tag{69e}$$

It is third order in κ and linear in Δ^2. If we insert $\Delta^2 = 1$ for the 1-axis and $\Delta^2 = f^2$ for the 2-axis into Eqs. (69), we re-obtain the solutions for $D = 0$ on the axes given above. However, this polynomial can not be factorized off the axes. But using κ as parameter, we can construct the shape of the critical curves and the caustics without numerical methods, although we are now faced with more complicated parameter ranges. These ranges can be found from the solutions on the axes. Figs.6,7,8 show the critical curves and the caustics in the case of an axis ratio of 0.8, and for b_c ranging between 0 and $f^{3/2}/2$, $f^{3/2}/2$ and $f^{3/2}/(1+f)$, and $f^{3/2}/(1+f)$ and $\sqrt{f}/(1+f)$, respectively. Figure 9 relates the parameter space of the NIE to the different possible topologies of the caustics.

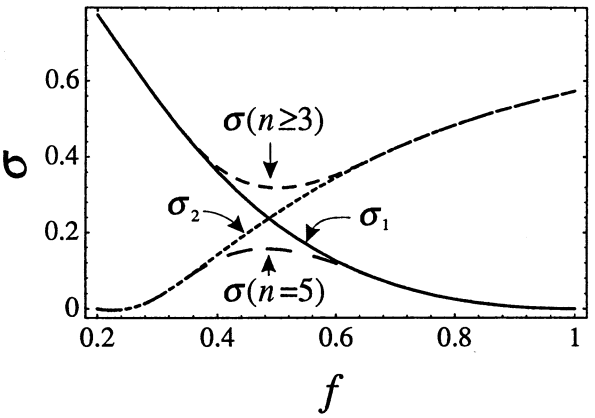

Fig. 11. Cross sections of the NIE for a given core radius $b_c = 0.1$. This corresponds to a physical core radius of about 0.5 kpc

4.2.4. Cross sections

Figure 10 shows some cross sections of the NIE. On the left side, we have plotted the cross sections of the second and the first caustic, on the right side the cross sections for multiple imaging and for five images; they were calculated numerically.

In Fig. 11 we show the behaviour of these cross sections for $b_c = 0.1$. This corresponds to a physical core radius of about half a kiloparsec, if we take typical values for lensing situations ($z_d \approx 0.5, z_s \approx 2, v \approx 220$km/s).

The cross sections for the second caustic and for multiple imaging depend only weakly on the ellipticity of the NIE, but strongly on the core radius, especially for very small b_c. Hence, the cut cross section of the SIE only yields a weak upper bound for the probability of multiple imaging. The strong dependency

of the second caustic on the core radius is easily understood, since the corresponding critical curve falls into a region of the lens plane which is strongly influenced by the core of the lens. In the above case ($b_c = 0.1$), the cross section for multiple imaging is less than 30 percent of that in the singular case. For larger ellipticity, a large fraction of this cross section is due to the first, and not to the second caustic. This is clearly seen in the upper row of Fig. 10, or for a special case in Fig. 11.

For the first caustic, the situation is reversed. The cross section depends sensitively on the axis ratio, but is a weaker function of the core radius if one excludes the cases of very large ellipticity and very large core radii. The argument is similar to the one given above: the first critical curve falls outside the region strongly influenced by the core. If we again take $b_c = 0.1$, we see that the cross section of the first caustic is about 90 percent of the caustic cross section of the SIE – except for very small f. The fact that the cross section for five images is also very sensitive to the core radius corresponds to the behaviour of the second caustic, which influences this cross section especially in the case of large b_c and small f.

5. Summary

We have presented a simple theory of lenses with elliptical mass distributions, following an 'isothermal' mass profile. These mass distributions are natural generalizations of spherical isothermal lenses often used in lens theory for modelling and lensing statistics. The deflection angle for the singular isothermal ellipsoid can be obtained from the Poisson Eq. (7) without employing the complex formalism. The explicit form for the deflection angle eliminates the need to perform an integral for the deflection (e.g., Bourassa & Kantowski 1975), and its real representation speeds up computations, due to the generally slow complex arithmetics on computers. The lens equation can be transformed into a one-dimensional form, making the inversion of the lens equation particularly simple. For nonsingular lenses, the deflection angle is somewhat more difficult, but can be written in closed form. It is derived (in the Appendix) using Wirtinger's calculus.

For both kinds of lenses, the critical curves have been calculated. They are quite trivial for the singular case, since they correspond to $\kappa = 1/2$, and slightly more complicated for the non-singular case. Nevertheless, also for the latter case, a classification of the caustic topologies can be derived (see Fig. 9). In addition, the area enclosed by the caustics has been calculated, and from that, cross sections for multiple imaging in its various image configurations have been derived.

In a forthcoming paper, we will apply our elliptical lens models to the gravitational lens system B1422+231 (Patnaik et al. 1992), which is likely to be due to a deflector with fairly large ellipticity (for an alternative view, see Hogg & Blandford 1993).

Acknowledgements. We would like to thank Jürgen Ehlers for helpful criticism and remarks during the course of this work, and we are grateful to the referee, Israel Kovner, for helpful discussions on the draft of this manuscript and for many useful remarks on the final version.

Appendix A: complex representation of lens theory

If we are dealing with elliptical mass distributions, it is convenient to use a complex representation of the lens theory. This was investigated by Bourassa & Kantowski (1975) and Bray (1984). In this appendix, we want to introduce the complex representation as we will use it, and we summarize the results of Bourassa & Kantowski in our notation.

If we write the vectors $\boldsymbol{x}$ and $\boldsymbol{y}$ in the lens and the source plane, respectively, and the deflection angle $\boldsymbol{\alpha}$ as complex numbers,

$$\begin{aligned} \mathrm{x} &= x_1 + \mathrm{i}x_2 = x\exp(\mathrm{i}\varphi) \quad , \\ \mathrm{y} &= y_1 + \mathrm{i}y_2 \quad , \\ \mathrm{a} &= \alpha_1 + \mathrm{i}\alpha_2 \quad , \end{aligned} \tag{A1}$$

we find as lens equation

$$\mathrm{y} = \mathrm{x} - \mathrm{a}(\mathrm{x}) \quad . \tag{A2}$$

The complex conjugate of the deflection angle a(x) is – as in the real case – given by an integration in the lens plane, namely

$$\mathrm{a}^*(\mathrm{x}) = \frac{1}{\pi}\int_{\mathbb{C}} \frac{\kappa(\mathrm{x}')}{\mathrm{x}-\mathrm{x}'}\, d^2x' \quad . \tag{A3}$$

We use Wirtinger's differential calculus here[3]. The operators

$$\frac{\partial}{\partial \mathrm{x}} := \frac{1}{2}\left(\frac{\partial}{\partial x_1} - \mathrm{i}\frac{\partial}{\partial x_2}\right) \quad , \tag{A4a}$$

$$\frac{\partial}{\partial \mathrm{x}^*} := \frac{1}{2}\left(\frac{\partial}{\partial x_1} + \mathrm{i}\frac{\partial}{\partial x_2}\right) \tag{A4b}$$

make it possible to apply the ordinary rules of partial differentiation to the (independent) complex variables x and x*. A complex function is analytic for those values of x where the partial derivative with respect to x* is vanishing. If we rewrite the deflection potential $\psi(\boldsymbol{x})$ in complex variables $\psi(\mathrm{x})$, namely

$$\psi(\mathrm{x}) := \frac{1}{\pi}\int_{\mathbb{C}} \kappa(\mathrm{x}')\ln|\mathrm{x}-\mathrm{x}'|\, d^2x' \quad , \tag{A5}$$

[3] To be mathematically rigorous we should construct the analytic continuation of a real-analytic function $f : \mathbb{R}^2 \to \mathbb{R}$ (or $\mathbb{C}$) , $(x_1, x_2) \mapsto f(x_1, x_2)$ into a complex-analytic function $\hat{f} : \mathbb{C}^2 \to \mathbb{R}$ (or $\mathbb{C}$) by defining

$$\hat{f}(\mathrm{x}, \overline{\mathrm{x}}) := f\left(\frac{\mathrm{x}+\overline{\mathrm{x}}}{2}, \frac{\mathrm{x}-\overline{\mathrm{x}}}{2\mathrm{i}}\right) \quad .$$

Wirtinger's differential operators are then taken to be the partial derivatives of $\hat{f}$ with respect to x and $\overline{\mathrm{x}}$, followed by the restriction $\overline{\mathrm{x}} = \mathrm{x}^*$. For simplicity, we write $f(\mathrm{x})$ instead of $\hat{f}(\mathrm{x}, \overline{\mathrm{x}})$.

we get the complex deflection angle from the equation

$$a^*(x) = 2\frac{\partial\psi}{\partial x} \quad . \tag{A6}$$

Poisson's equation corresponds to

$$2\frac{\partial^2\psi}{\partial x\,\partial x^*} = \frac{\partial a^*}{\partial x^*} = \kappa \quad . \tag{A7}$$

Therefore a^* is analytic if, and only if, κ vanishes. Fermat's potential is given by

$$\Phi(x, y) = \frac{1}{2}(x - y)(x - y)^* - \psi(x) \quad . \tag{A8}$$

The lens equation can therefore be written as gradient mapping,

$$\frac{\partial\Phi}{\partial x^*} = 0 \quad . \tag{A9}$$

We also define a complex shear, $\Gamma := \gamma_1 + i\gamma_2$, which can be shown to be

$$\Gamma(x) = \left(\frac{\partial a^*}{\partial x}\right)^* \quad . \tag{A10}$$

If we write the absolute value of the shear as γ, we get the usual expression for the magnification, $\mu = 1/D$ with $D := (1 - \kappa)^2 - \gamma^2$. In Sect.4, we used the mapping of a vector $\boldsymbol{T}$ from the lens to the source plane. In the real representation, this is done by the linear mapping $A \cdot \boldsymbol{T}$. It is easy to check that this corresponds to the complex expression $(1 - \kappa)T - \Gamma^*T^*$.

We introduce now non-orthogonal, elliptical coordinates b and θ by $x =: b\cos\theta + i(b/f)\sin\theta$ for the description of elliptical lens models. Due to $b^2 = x_1^2 + f^2x_2^2 = f'^2(x^2 + x^{*2})/4 + (1 + f^2)x\,x^*/2$, b is the minor axis (for $f \leq 1$) of an iso-density ellipse and corresponds to Eq.(21d). If we rewrite Eq.(A3) in these new coordinates, the angular integral can be done (Bourassa & Kantowski 1975), leading to

$$a^*(x) = 2\int_0^{b(x)} \frac{b'\kappa(b')}{\sqrt{f^2x^2 + f'^2b'^2}}\,db' \quad , \tag{A11}$$

where $\sqrt{f^2x^2 + f'^2b'^2}$ is defined as the continous continuation of $\sqrt{f^2x^2} = fx$ with respect to b'.

Bourassa & Kantowski have also shown that the deflection angle is determined solely by the mass within the iso-density ellipse given by this position. These equations have been used in this work for the calculation of the NIE and for the complex description of the SIE.

Appendix B: isothermal lens models in complex representation

In this appendix we give some details of the calculations in complex representation for the singular as well as for the non-singular case.

The singular case

Inserting the surface mass density of the SIE, Eq.(21b), into Eq.(A11), we find for the deflection angle of this model

$$a^*(x) = \frac{\sqrt{f}}{f'}\operatorname{arsinh}\frac{f'b}{fx} \quad . \tag{B1}$$

Using the relation $\sigma + i\tau = \operatorname{arsinh}(s + it)$, where $s := \sinh\sigma\cos\tau$ and $t := \cosh\sigma\sin\tau$, we have checked the equivalence of Eqs.(27a) and (B1).

For the SIE in complex representation we find

$$\kappa = \frac{\partial a^*}{\partial x^*} = \frac{\sqrt{f}}{2b}\frac{1}{\sqrt{f^2x^2 + f'^2b^2}}\frac{\partial b^2}{\partial x^*} \quad . \tag{B2}$$

This leads to a very useful relation, namely $(b^2)_{,x^*} = x_1 + if^2x_2 = \sqrt{f^2x^2 + f'^2b^2}$. In this equation we used the index separated by a comma to denote Wirtinger's differentiation. With the help of this equation we can simplify the expression for the shear of the SIE,

$$\Gamma^*(x) = \frac{\partial a^*}{\partial x} = -\frac{\sqrt{f}}{(b^2)_{,x^*}}\frac{2b^2 - x(b^2)_{,x}}{2b\,x} = -\kappa\frac{x^*}{x} \quad . \tag{B3}$$

For the last equality we used $2b^2 - x(b^2)_{,x} = x^*(b^2)_{,x^*}$, which can be checked by calculating the two components separately. Of course, the complex shear is identical to the real one due to $\Gamma = -\kappa\,x/x^* = -\kappa\,\exp(2i\varphi) = -\kappa\big[\cos(2\varphi) + i\sin(2\varphi)\big] = \gamma_1 + i\gamma_2$.

The non-singular case

If we integrate Eq.(A11) with Eq.(22b) inserted, we obtain the result:

$$a^*(x) = \frac{\sqrt{f}}{f'}\left[\operatorname{arsinh}\left(\Xi\sqrt{b^2 + b_c^2}\right) - \operatorname{arsinh}\left(\Xi\,b_c\right)\right] \tag{B4a}$$

$$= \frac{\sqrt{f}}{f'}\left[\operatorname{artanh}\frac{f'\sqrt{b^2 + b_c^2}}{(b^2)_{,x^*}} - \operatorname{artanh}\frac{f'b_c}{fx}\right] \quad . \tag{B4b}$$

In Eq.(B4a), we have used

$$\Xi(x) := \frac{f'}{\sqrt{f^2x^2 - f'^2b_c^2}} \quad .$$

For $b_c = 0$, we get $\Xi(x) = f'/(fx)$, and we end up with the complex deflection angle of the SIE. It is possible, although very cumbersome, to split the complex deflection angle of the SIE into the real and the imaginary part, using the relations $\operatorname{artanh} z = (1/2)\ln[(1 + z)/(1 - z)]$ and $\ln z = \ln|z| + i\arg z$. The results are given in Eqs.(62).

The complex shear, as it is defined in App.A, is given by the equations

$$\Gamma^*(x) = \frac{\partial a^*}{\partial x}$$
$$= \kappa\frac{(b^2)_{,x}}{(b^2)_{,x^*}} + \frac{f^{3/2}}{f^2x^2 - f'^2b_c^2}\left(b_c - \frac{fx\sqrt{b^2 + b_c^2}}{(b^2)_{,x^*}}\right) \tag{B5a}$$

$$= \frac{\sqrt{f}}{f^2 x^2 - f'^2 b_c^2} \times \left[\frac{\kappa}{\sqrt{f}} (b^2)_{,x} (b^2)_{,x^*} - \frac{1+f^2}{2} \sqrt{b^2 + b_c^2} + f b_c \right] \quad . \tag{B5b}$$

In Eqs.(63), we have decomposed this result into γ_1 and γ_2.

References

Binney, J., Tremaine, S., 1987, Galactic Dynamics, Princeton Series in Astrophysics

Blandford, R. D., Narayan, R., 1986, ApJ 310, 568.

Blandford, R. D., Kochanek, C. S., 1987, ApJ 321, 658.

Bourassa, R. R., Kantowski, R., Norton, T. D., 1973, ApJ 185, 747.

Bourassa, R. R., Kantowski, R., 1975, ApJ 195, 13.

Bourassa, R. R., Kantowski, R., 1976, ApJ 205, 674.

Bray, I., 1984, MNRAS 208, 511.

Chang, K., Refsdal, S., 1979, Nat 282, 561.

Chang, K., Refsdal, S., 1984, A&A 132, 168.

Falco, E. E., Gorenstein, M. V., Shapiro, I. I., 1985, ApJ 289, L1.

Falco, E. E., Gorenstein, M. V., Shapiro, I. I., 1991, ApJ 372, 364.

Gradshteyn, I. S., Ryzhik, I. M., 1980, Table of integrals, series and products, Academic Press

Hogg, D. W., Blandford, R. D., 1993, Caltech preprint

Kassiola, A., Kovner, I., 1993, Ap.J., in press

Kochanek, C. S., Blandford, R. D., 1987, ApJ 321, 676.

Kochanek, C. S., Blandford, R. D., Lawrence, C. R., Narayan, R., 1989, MNRAS 238, 43.

Kochanek, C. S., 1991a, ApJ 373, 354.

Kochanek, C. S., 1991b, ApJ 382, 58.

Kovner, I., 1987a, ApJ 312, 22.

Kovner, I., 1987b, Nat 325, 507.

Kovner, I., 1987c, ApJ 316, 52.

Mao, S., 1992, ApJ 389, 63.

Mestel, L., 1963, MNRAS 126, 553.

Narasimha, D., Subramanian, K., Chitre, S. M., 1982, MNRAS 200, 941.

Patnaik, A. R., Browne, I. W. A., Walsh, D., Chaffee, F. H., Foltz, C. B., 1992, MNRAS 259, 1P.

Schneider, P., Ehlers, J., Falco, E. E., 1992, Gravitational Lensing, Astronomy and Astrophysics Series, Springer-Verlag (SEF)

Schneider, P., Weiss, A., 1991, A&A 247, 269.

Schneider, P., Weiss, A., 1992, A&A 260, 1.

Schramm, T., 1990, A&A 231, 19.

Turner, E. L., Ostriker, J. P., Gott, J. R., 1984, ApJ 284, 1.

Young, P., Deverill, R. S., Gunn, J. E., Westphal, J. A., Kristian, A., 1981a, ApJ 244, 723.

Young, P., Gunn, J. E., Kristian, J., Oke, J. B., Westphal, J. A. 1981b, ApJ 244, 736.

This article was processed by the author using Springer-Verlag TEX A&A macro package 1992.